
Flow Matching for Geometric Trajectory Simulation

Kiet Bennema ten Brinke

Department of Mathematics and Computer Science
Eindhoven University of Technology
Eindhoven, The Netherlands
kiettenbrinke@gmail.com

Koen Minartz

Department of Mathematics and Computer Science
Eindhoven University of Technology
Eindhoven, The Netherlands
k.minartz@tue.nl

Vlado Menkovski

Department of Mathematics and Computer Science
Eindhoven University of Technology
Eindhoven, The Netherlands
v.menkovski@tue.nl

Abstract

The simulation of N-body systems is a fundamental problem with applications in a wide range of fields, such as molecular dynamics, biochemistry, and pedestrian dynamics. Machine learning has become an invaluable tool for scaling physics-based simulators and developing models directly from experimental data. In particular, recent advances based on deep generative modeling and geometric deep learning have enabled probabilistic simulation by modeling complex distributions over trajectories while respecting the permutation symmetry that is fundamental to N-body systems. However, to generate realistic trajectories, existing methods must learn complex transformations starting from uninformed noise and do not allow for the exploitation of domain-informed priors. In this work, we propose STFlow to address this limitation. By leveraging flow matching and data-dependent couplings, STFlow facilitates physics-informed simulation of geometric trajectories without sacrificing model expressivity or scalability. Our evaluation on N-body dynamical systems, molecular dynamics, and pedestrian dynamics benchmarks shows that STFlow produces significantly lower prediction errors while enabling more efficient inference, highlighting the benefits of employing physics-informed prior distributions in probabilistic geometric trajectory modeling.

1 Introduction

N-body simulations model the dynamical interactions of multiple individual particles and play an important role in computational science at all physical scales, ranging from astrophysics (Heggie, 2003; Bédorf, 2014) to molecular dynamics (Thompson et al., 2022). These simulations predict the evolution of complex interacting systems, enabling the testing of fundamental theories, understanding emergent phenomena from intricate interactions, and exploring scenarios that are experimentally inaccessible and too complex for analytical solutions. Machine learning methods play an important role in scaling the computational complexity of traditional N-body models (Cuesta-Lazaro and Mishra-Sharma, 2024), as well as in producing simulations directly from empirical observations, entirely bypassing the need for a known physics-based model (Mottaghi et al., 2016; Cranmer et al., 2020; Minartz et al., 2025).

Any model capable of successfully predicting N-body trajectories needs to capture temporal dependencies as well as interactions between bodies: the evolution of a particle’s trajectory is dependent

on the past states of itself as well as those of its neighbors. These dependencies are additionally modulated by the geometric structure and topology of the data (Gravina and Bacciu, 2024). Further complicating the modeling task, many real-life N-body systems are subject to stochastic effects, affected by unobserved variables, or are exponentially diverging in certain regions of the phase space. In these cases, we need a probabilistic model that expresses a distribution over the trajectories of all nodes, rather than modeling point estimates.

A common modeling approach is to autoregressively factorize the aforementioned distribution over time, where the prediction of a particle’s state is informed by current and past states of itself and its neighbors through a geometrically informed model that is applied iteratively. However, this iterative sampling process generally accumulates errors (Sanchez-Gonzalez et al., 2020; Brandstetter et al., 2022b) and is inefficient for inference, as the autoregressive generation process is sequential and not amenable to parallelization (Van Den Oord et al., 2016; Hoogeboom et al., 2022).

Alternatively, diffusion models (Ho et al., 2020; Sohl-Dickstein et al., 2015) enable parallelized generation and training, and have recently shown promising results as a generative modeling approach for high-dimensional temporal data, e.g. video (Ho et al., 2022) and dynamical systems described by partial differential equations (Kohl et al., 2024; Shysheya et al., 2024; Lippe et al., 2023; Cachay et al., 2023; Ruhe et al., 2024; Shehata et al., 2025; Pedersen et al., 2025). Still, for N-body systems, such a model must not only capture the complex temporal correlations, but also the dependencies on all neighboring particles while respecting the permutation symmetry that is fundamental to all particle-based simulations. In addition, the task of learning a mapping from the prior distribution to the highly complex data distribution remains challenging, especially considering the many possible relative permutations that need to be considered to couple prior and data samples (Klein et al., 2023). Simultaneously, a wealth of knowledge on characteristics of the trajectory data is typically available, which nevertheless remains unexploited in current approaches.

In this work, we introduce Spatio-Temporal Flow (STFlow) to address this gap. STFlow is a probabilistic geometric trajectory simulation model based on *flow matching* (Lipman et al., 2023). STFlow improves simulation accuracy by drastically simplifying the mapping between the prior and data distributions while maintaining the scalability of diffusion-based approaches. Our main contributions are summarized as follows:

- We introduce STFlow, a data-driven simulator that learns a permutation-invariant probability distribution over the dynamics of a set of particles. STFlow utilizes convolutional and message passing neural network components to effectively model spatio-temporal dependencies while respecting the permutational symmetry fundamental to all N-body dynamical systems.
- We propose a simple yet effective prior distribution for geometric trajectory data. By constructing the prior as a random walk with parameters estimated from the trajectory’s initial observed timesteps, the resulting samples are naturally coupled during training, which allows for effective learning of a straighter flow from prior to data.
- We evaluate our approach on three challenging datasets: a synthetic physics-based N-body system dataset, pedestrian trajectory forecasting, and molecular dynamics simulation. Our results show that STFlow outperforms the existing state-of-the-art for these challenging benchmarks in most cases. Moreover, we investigate the importance of the physics-informed prior and architectural design choices, and find that these are key drivers of the observed performance improvements.

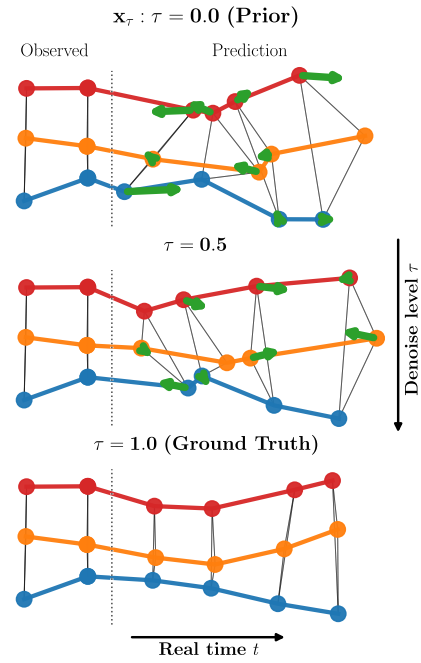


Figure 1: STFlow generates trajectories by sampling from a physics-informed prior and learning a vector field (green arrows).

2

2 Related Work

Early work in the domain of neural network-driven geometric trajectory simulation generally used models based on autoregressive Graph Neural Networks (GNNs), as they align with the permutation-symmetric nature of the problem [Battaglia et al. \(2016\)](#); [Kipf et al. \(2018\)](#); [Sanchez-Gonzalez et al. \(2020\)](#). Since then, various architectural and modeling advances have been proposed,

for example focusing on continuous-time dynamics through Neural ODEs [Gupta et al. \(2022\)](#); [Luo et al. \(2023, 2024\)](#), the incorporation of symmetry constraints [Satorras et al. \(2021\)](#); [Thomas et al. \(2018a\)](#); [Brandstetter et al. \(2022a\)](#); [Fuchs et al. \(2020\)](#); [Ruhe et al. \(2023\)](#); [Bekkers et al. \(2024\)](#), or on interpretability through symbolic methods [Cranmer et al. \(2020\)](#); [Lemos et al. \(2023\)](#).

Although the above methods are relevant to geometric trajectory simulation, many real-life systems are stochastic or otherwise do not lend themselves to point prediction methods, for example due to their chaotic nature. Consequently, recent works have proposed probabilistic simulation methods based on generative models. We distinguish two main categories of approaches. First, autoregressive probabilistic models generate trajectories through a recurrent time-stepping approach, factorizing the distribution over trajectories $p(x^{0:T})$ as $p(x^0) \prod_{t=1}^T p(x^t | x^{0:t})$ [Salinas et al. \(2020\)](#); [Salzmann et al. \(2021\)](#); [Gupta et al. \(2018\)](#); [Amirian et al. \(2019\)](#); [Xu et al. \(2022\)](#); [Yildiz et al. \(2022\)](#); [Minartz et al. \(2023\)](#); [Wu et al. \(2024\)](#). Intuitively, this is similar to physics-based numerical methods that evolve the state of the system over time. Although such time-stepping approaches are in principle capable of real-time generation of indefinitely long trajectories, they suffer from error accumulation as the simulation horizon increases [Sanchez-Gonzalez et al. \(2020\)](#); [Brandstetter et al. \(2022b\)](#); [Minartz et al. \(2023\)](#); [Lippe et al. \(2023\)](#) and are difficult or impossible to parallelize during both training and inference, limiting their scalability. More recently, generative approaches that generate the trajectory as a whole have gained traction, with diffusion-based models being the most popular approach [Gu et al. \(2022a\)](#); [Xu et al. \(2023\)](#); [Mao et al. \(2023\)](#); [Wen et al. \(2023\)](#); [Han et al. \(2024\)](#). However, these models need to learn a complicated mapping from uninformed Gaussian noise to realistic trajectory data, and lack inductive biases related to trajectories such as continuity and inertia. In contrast, STFlow leverages a physics-informed prior that already captures such basic properties, thereby simplifying the training and inference procedure.

3 STFlow: generative modeling of geometric trajectories

3.1 Problem formulation

Geometric trajectories. We represent a geometric trajectory as $\mathcal{G} := (\mathbf{x}, \mathbf{h}, \mathcal{E})$, where $\mathbf{x} := \mathbf{x}^{0:T} := \{[\mathbf{x}_{(i)}^0, \dots, \mathbf{x}_{(i)}^{T-1}]\}_{i=0}^N \in \mathbb{R}^{T \times N \times d}$ is a set of N objects containing the sequence of their coordinates in d dimensional space over T timesteps, $\mathbf{h} := \{[\mathbf{h}_{(i)}^0, \dots, \mathbf{h}_{(i)}^{T-1}]\}_{i=0}^N \in \mathbb{R}^{T \times N \times h}$ are node features with dimensionality h that serve as model input, and \mathcal{E} is the set of edges defining the interaction structure between the objects within the same timestep; in case the interaction structure is not known, one can assume a fully connected graph. c is the number of initial frames that are observed and serve as input to the simulation model, and $f := T - c$ is the number of target frames.

Goal and approach. Our goal is to train a data-driven simulation model by learning the joint probability distribution over trajectories \mathbf{x} from the ground truth distribution p_1 :

$$p_1(\mathbf{x} | \mathbf{h}, \mathcal{E}) = p_1(\mathbf{x}^{c:T} | \mathbf{h}, \mathcal{E}, \mathbf{x}^{0:c}) p_1(\mathbf{x}^{0:c} | \mathbf{h}^{0:c}, \mathcal{E}^{0:c}) \quad (1)$$

In the simulation problem setting, we presuppose that an initial part of the trajectory $\mathbf{x}^{0:c}$ is provided to the model as initial conditions, such that we can readily obtain samples from the ground truth $p_1(\mathbf{x}^{0:c} | \mathbf{h}^{0:c}, \mathcal{E}^{0:c})$. Consequently, the machine learning task boils down to learning the distribution over future timesteps $p_1(\mathbf{x}^{c:T} | \mathbf{h}, \mathcal{E}, \mathbf{x}^{0:c})$.

In principle, our approach allows for values of c located at arbitrary points in time within the trajectories. This includes no observed frames ($c = 0$), specifying unconditional generation, and observing the first $c = T - 1$ frames, possibly applied iteratively for an *autoregressive* style of generation. Alternatively, the formulation can even be modified to support conditioning on future frames to recover earlier observations. In this work we limit ourselves to the causal forward-temporal formulation, with c fixed for each dataset.

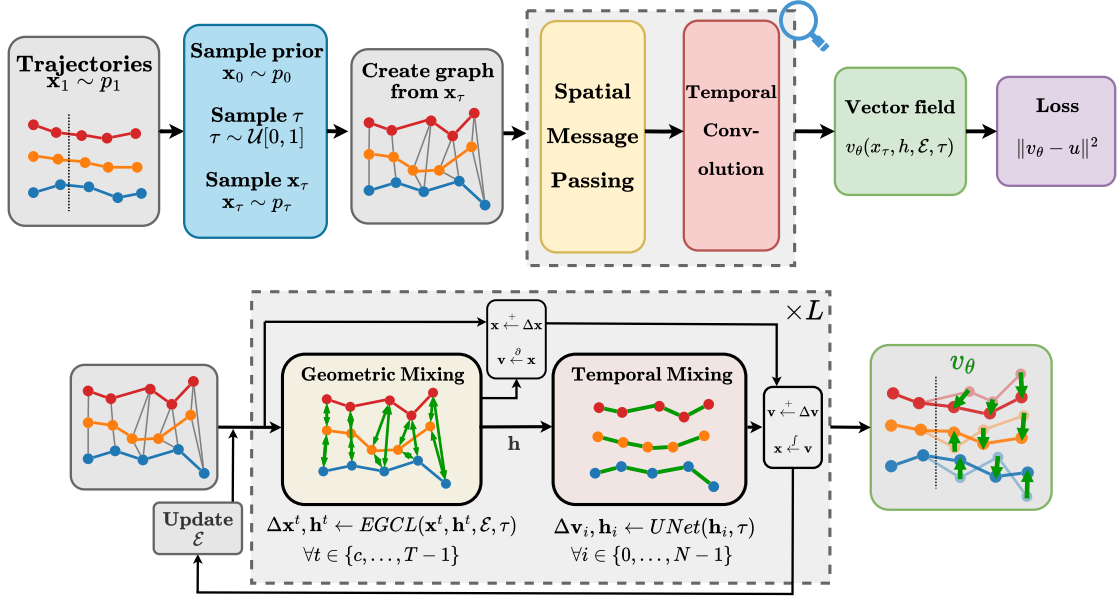


Figure 2: Overview of STFlow. Given trajectories $\mathbf{x}_1 \sim p_1$, we construct a noisy prior \mathbf{x}_0 informed by the observed initial conditions and predict a vector field v_θ using repeating layers of spatial message passing and temporal convolution.

We approach this problem by leveraging flow matching Lipman et al. (2023). Flow matching involves training a model v_θ to approximate a ground truth time-dependent *vector field* $u : \mathbb{R}^{T \times N \times d} \times [0, 1] \rightarrow \mathbb{R}^{T \times N \times d}$. This vector field defines a *flow* ψ from a known prior distribution p_0 to the target data distribution p_1 . The flow is distributed according to a *probability path* $(p_\tau)_{0 \leq \tau \leq 1}$, from which we can sample trajectories \mathbf{x}_τ that flow from the prior to the target distribution. In order to generate a sample from the learned target distribution p_1 , we sample noisy trajectories $\mathbf{x}_0 \sim p_0$ from the prior, and then solve the Ordinary Differential Equation (ODE) $d\mathbf{x} = v_\theta(\mathbf{x}, \mathbf{h}, \mathcal{E}, \tau) d\tau$ determined by the learned vector field v_θ . We visualize an example of three trajectories \mathbf{x}_τ with three different noise levels $\tau \in \{0, 0.5, 1\}$, together with v_θ as green arrows, in Figure 1.

3.2 Flow Matching with data-dependent coupling

Data-dependent couplings for temporal simulation In order to train our model, we have to draw samples $(\mathbf{x}_0, \mathbf{x}_1) \sim \pi$ from some coupling π of the source distribution p_0 and target distribution p_1 . The simplest option would be to draw these pairs independently, i.e. $\pi = p_0(\mathbf{x}_0)p_1(\mathbf{x}_1)$, with p_0 being a simple uninformed distribution such as a standard Gaussian. However, this approach would ignore the fact that there is a natural coupling present in our problem setting. Instead, we define p_0 through a *data-dependent coupling* $\pi(\mathbf{x}_0, \mathbf{x}_1) = \pi(\mathbf{x}_0 \mid \mathbf{x}_1)p_1(\mathbf{x}_1)$ (Albergo et al., 2024). Such a data-dependent coupling defines a prior density $\int_{\mathbf{x}_1} \pi(\mathbf{x}_0 \mid \mathbf{x}_1)p_1(\mathbf{x}_1) d\mathbf{x}_1$ over \mathbf{x}_0 . Let $\pi(\mathbf{x}_0 \mid \mathbf{x}_1)$ be of the form $\mathbf{x}_0 = m(\mathbf{x}_1) + \zeta$, where $m : \mathbb{R}^{T \times N \times d} \rightarrow \mathbb{R}^{T \times N \times d}$ is a function that corrupts \mathbf{x}_1 and ζ is a stochastic variable that is conditionally independent of \mathbf{x}_1 given $m(\mathbf{x}_1)$. Following the factorization of Equation 1, we choose $m(\mathbf{x}_1) = [\mathbf{x}_1^0, \dots, \mathbf{x}_1^{c-1}, \mathbf{0}, \dots, \mathbf{0}]$ and $\zeta = [\mathbf{0}, \dots, \mathbf{0}, \zeta^c, \dots, \zeta^{T-1}]$. Intuitively, this boils down to a prior in which the c initial observations remain intact in \mathbf{x}_0 , while the to-be-simulated part of the trajectory is replaced with stochastic variables ζ^t .

Physics-informed prior The most straightforward choice for a distribution over ζ , and also the one used in Albergo et al. (2024), would be a multivariate Gaussian $\mathcal{N}(0, \Sigma)$. However, the flow ψ from $p_0(\mathbf{x}_0)$ to $p_1(\mathbf{x}_1)$ is easier to learn when the *transport cost* is minimized (Tong et al., 2023; Albergo et al., 2024). To achieve this, we require a prior p_0 which **1.** incorporates trajectory-specific characteristics to reduce transport cost via initializations that are closer to \mathbf{x}_1 ; **2.** is computationally efficient to sample from; and **3.** is conditionally independent of $\mathbf{x}_1^{c:T}$ given $m(\mathbf{x}_1)$. With this in mind, and with $\mathbf{x}_0 := [\mathbf{x}_1^0, \dots, \mathbf{x}_1^{c-1}, \zeta^c, \dots, \zeta^{T-1}]$ we choose $\zeta \in \mathbb{R}^{f \times N \times d}$ to be distributed as follows:

$$\begin{aligned} \zeta^t &= \zeta^{t-1} + \mu + \sigma_o \odot \mathbf{z}^t & \forall t \in \{c, \dots, T-1\}, \\ \zeta^{c-1} &= \mathbf{x}^{c-1}, \end{aligned} \tag{2}$$

where $\mu = \frac{1}{c-1} \sum_{t=1}^{c-1} (\mathbf{x}^t - \mathbf{x}^{t-1})$, $\sigma_o = \frac{1}{c-1} \sum_{t=1}^{c-1} \|\mathbf{x}^t - \mathbf{x}^{t-1} - \mu\|^2 \cdot s$ with $\mu, \sigma_0 \in \mathbb{R}^{N \times d}$, where s is a hyperparameter controlling the amount of noise in p_0 , \odot denotes element-wise multiplication, and $\mathbf{z}^t \sim \mathcal{N}(\mathbf{0}, \mathbf{I})$. Intuitively, ζ as defined in Equation 2 follows a random walk of which the parameters are fitted to the initial observed part of each node's trajectory. As such, this random walk obeys basic physical properties of trajectories, such as continuity and inertia, resulting in prior samples that already resemble real trajectories and thus expedite the learning process by reducing the transport cost.

Training The conditional flow matching training objective consists of *matching* the flows by training the vector field v_θ using Mean Squared Error (MSE) (Lipman et al., 2023). We assume linear Gaussian probability paths, such that $\mathbf{x}_\tau \sim p_\tau := \mathcal{N}(\mathbf{x} \mid \tau \mathbf{x}_1 + (1 - \tau) \mathbf{x}_0, \sigma_p^2)$. This allows the vector field u to take the simple form of $u = \mathbf{x}_1 - \mathbf{x}_0$ (Tong et al., 2023). In our case, the loss \mathcal{L}_{CFM} is defined as:

$$\mathcal{L}_{CFM}(\theta) = \mathbb{E}_{\tau, \mathbf{x}_0, \mathbf{x}_1} \|v_\theta(\mathbf{x}_\tau, \mathbf{h}, \mathcal{E}, \tau) - (\mathbf{x}_1 - \mathbf{x}_0)\|^2, \quad (3)$$

where $\tau \sim \mathcal{U}[0, 1]$, $\mathbf{x}_1 \sim p_1$, $\mathbf{x}_0 = m(\mathbf{x}_1) + \zeta$, and $\mathbf{x}_\tau \sim p_\tau$. During training, we provide our model with the mask indicating which frames are considered observed, which is used for generating \mathbf{x}_0 . We ignore the output of v_θ at timesteps $t \in [0, c-1]$, as we only predict the parts of the trajectories which are not already observed. Our approach also allows for training with varying observed window size $c \sim \mathcal{U}[0, T-1]$, such that trajectories can be sampled both unconditionally or with any amount of observed timesteps, without additional retraining or guidance needed. A detailed description of the training procedure is denoted in A.1.

Inference We sample noisy trajectories from the prior $\mathbf{x}_0 \sim p_0$ and integrate the vector field $v_\theta(\mathbf{x}_\tau, \mathbf{h}, \mathcal{E}, \tau)$ using the Euler integration method using 50 function evaluations (NFEs) to simulate trajectories $\mathbf{x}^{c:T}$ given $\mathbf{x}^{0:c}$ as initial conditions. This is presented in A.1 for more detail.

3.3 Model Architecture

The two main building blocks of the architecture for $v_\theta(\mathbf{x}, \mathbf{h}, \mathcal{E}, \tau)$ are the *Spatial message passing* (SMP) layer and the *Temporal convolution* (TC) layer. Generally, interactions among the nodes are governed by the relative positioning of nodes, whereas the temporal correlation affects the increments between subsequent positions in translation-symmetric systems. Consequently, we let the SMP layer operate on positions, while the TC layer operates on velocities. The trajectory $\mathbf{x}^{c:T}$ and hidden representation \mathbf{h} are updated after each layer, allowing each layer to make residual-style denoising modifications to the trajectory in the real geometric space, similar to Han et al. (2024). Additionally, the connectivity and edge features \mathcal{E} are updated after each TC layer to present subsequent SMP layers with more informative edge features. Both layers are given an encoding of τ as input, as is common in diffusion and flow matching models. A schematic of our architecture can be seen in Figure 2.

Our SMP layer is based on the Equivariant graph convolutional layer (EGCL) by Satorras et al. (2021), which captures spatial interactions by aggregating learned messages along the edges. The layer is defined as $\Delta \mathbf{x}^t, \mathbf{h}^t \leftarrow \text{EGCL}(\mathbf{x}^t, \mathbf{h}^t, \mathcal{E}^t, \tau)$, updating the positions and node features. The message passing is carried out independently for each timestep $t \in [c, T-1]$. The aim of the EGCL layer is to fuse the geometric information contained in the graph, informing nodes of their neighborhood.

The temporal convolution is carried out by a UNet, based on the architecture of Dhariwal and Nichol (2021) designed for diffusion on images and allowing for conditioning on noise level τ . We define it as $\Delta \mathbf{v}^{c:T}, \mathbf{h} \leftarrow \text{UNet}(\mathbf{h}, \tau)$. The function of the UNet is to capture the dynamics of individual trajectories and to propagate information in earlier timesteps towards later timesteps. More details about the SMP and TC layers can be found in A.2. By alternating and stacking both spatial and temporal aggregation layers we enable the model to effectively capture and integrate complex spatio-temporal dependencies across the trajectory, resulting in a more accurate vector field approximation.

4 Experiments

We demonstrate the performance of STFlow on N-body physical simulation (§4.1.1), molecular dynamics (§4.1.2) and pedestrian trajectory forecasting (§4.1.3) to show that our model can be applied across multiple domains of the conditional trajectory prediction setting. We evaluate on velocity and

Table 1: Conditional Generation on N-Body systems, averaged over 5 runs.

	Gravity		Spring		Charged	
	ADE	FDE	ADE	FDE	ADE	FDE
Prior	1.591	3.101	0.2312	0.5083	0.526	1.013
TFN	0.327	0.761	0.1013	0.2364	0.330	0.754
SE(3)-Tr	0.338	0.830	0.0865	0.2043	0.395	0.936
EGNN	0.310	0.709	0.0101	0.0231	0.186	0.426
SVAE	0.582	1.101	0.0120	0.0209	0.378	0.732
EqMotion	0.302	0.671	0.0134	0.0358	0.141	0.310
GeoTDM	0.256	0.613	0.0030	0.0079	0.110	0.258
STFlow	0.115	0.245	0.0002	0.0004	0.093	0.172

Table 2: Conditional Generation of Pedestrian Trajectories from ETH-UTY dataset ($min_{20}\text{ADE}/min_{20}\text{FDE}$).

	ETH	Hotel	Univ	Zara1	Zara2	Mean
Prior	0.91/1.88	0.24/0.46	0.66/1.35	0.47/1.00	0.38/0.79	0.53/1.10
Linear	1.07/2.28	0.31/0.61	0.52/1.16	0.42/0.95	0.32/0.72	0.53/1.14
SGAN	0.64/1.09	0.46/0.98	0.56/1.18	0.33/0.67	0.31/0.64	0.46/0.91
PECNet	0.54/0.87	0.18/0.24	0.35/0.60	0.22/0.39	0.17/0.30	0.29/0.48
Traj++	0.54/0.94	0.16/0.28	0.28/0.55	0.21/0.42	0.16/0.32	0.27/0.50
BiTraP	0.56/0.98	0.17/0.28	0.25/0.47	0.23/0.45	0.16/0.33	0.27/0.50
MID	0.50/0.76	0.16/0.24	0.28/0.49	0.25/0.41	0.19/0.35	0.27/0.45
SVAE	0.47/0.76	0.14/0.22	0.25/0.47	0.20/0.37	0.14/0.28	0.24/0.42
GeoTDM	0.46/0.64	0.13/0.21	0.24/0.45	0.21/0.39	0.16/0.30	0.23/0.40
STFlow	0.50/0.74	0.20/0.29	0.42/0.68	0.20/0.31	0.18/0.28	0.30/0.46

Table 3: Conditional Generation of atom trajectories from MD17 dataset, averaged over 5 runs.

	Aspirin		Benzene		Ethanol		Malonaldehyde		Naphthalene		Salicylic		Toluene		Uracil	
	ADE	FDE	ADE	FDE	ADE	FDE	ADE	FDE	ADE	FDE	ADE	FDE	ADE	FDE	ADE	FDE
Prior	0.513	0.848	0.285	0.459	0.706	1.207	0.502	0.831	0.468	0.728	0.474	0.755	0.540	0.840	0.462	0.737
TFN	0.133	0.268	0.024	0.049	0.201	0.414	0.184	0.386	0.072	0.098	0.115	0.223	0.090	0.150	0.090	0.159
SE(3)-Tr	0.294	0.556	0.027	0.056	0.188	0.359	0.214	0.456	0.069	0.103	0.189	0.312	0.108	0.184	0.107	0.196
EGNN	0.267	0.564	0.024	0.042	0.268	0.401	0.393	0.958	0.095	0.133	0.159	0.348	0.207	0.294	0.154	0.282
SVAE	0.301	0.428	0.114	0.133	0.387	0.505	0.287	0.430	0.124	0.135	0.122	0.142	0.145	0.171	0.145	0.156
EqMotion	0.185	0.246	0.029	0.043	0.152	0.247	0.155	0.249	0.073	0.092	0.110	0.151	0.097	0.129	0.088	0.116
GeoTDM	0.107	0.193	0.023	0.039	0.115	0.209	0.107	0.176	0.064	0.087	0.083	0.120	0.083	0.121	0.074	0.099
STFlow	0.086	0.158	0.014	0.022	0.079	0.141	0.076	0.138	0.023	0.038	0.043	0.072	0.036	0.059	0.058	0.090

acceleration densities of the simulated trajectories (§4.2), show the performance and efficiency of our approach for different inference parameters (§4.3) and ablate on core design choices (§4.4). Unless otherwise indicated, we follow the experimental setups of Han et al. (2024) in §4.1 to ensure a fair comparison between the most recent relevant geometric trajectory generation models; we redescribe these setups in §4.1 for completeness. Additionally, the conditional generation results in Tables 1, 2 and 3 except for those of our own approach and ablations thereof are taken from Han et al. (2024). We report the standard deviations of the results in Table 1, 2 and 3 in A.5, hyperparameters used for training in A.3, used compute resources in A.4 and additional density evaluations and trajectory visualizations in A.6.

4.1 Conditional trajectory generation

4.1.1 N-body systems

Datasets and setup We use three different kinds of simulated N-body systems, each with different forces acting on the particles. **1. Gravity System** (Brandstetter et al., 2022a) with $N = 10$ particles, each having a random mass and initial velocity influenced by gravitational forces. **2. Spring Dynamics** (Kipf et al., 2018) containing $N = 5$ particles with random mass which are connected by springs with a probability of 0.5 between pairs, where the springs abide by Hooke’s Law. **3. Charged Particles** (Kipf et al., 2018; Satorras et al., 2021) where $N = 5$ particles with random charges of -1 or $+1$ are driven by the Coulomb force. All trajectories have a total length of $T = 30$ with a conditioning window of $c = 10$. For all three datasets the split consists of 3000 training, 2000 validation and 2000 testing samples.

Baselines We look at three different kinds of approaches. Frame-to-frame prediction models: Tensor field networks (Thomas et al., 2018b), SE(3)-Transformers (Fuchs et al., 2020) and EGNN (Satorras et al., 2021); Deterministic trajectory models: Eqmotion (Xu et al., 2023) and Probabilistic trajectory models: SVAE (Xu et al., 2022) and GeoTDM (Han et al., 2024). To put the results into perspective, we additionally report the metrics when sampling from our prior p_0 , defined by Eq. 2, and using those samples directly as predictions.

Metrics As often used in trajectory forecasting literature, we look at the Average Displacement Error (ADE) and Final Displacement Error (FDE) to measure performance. ADE is defined as $ADE(\mathbf{x}^{c:T}, \mathbf{y}^{c:T}) = \frac{1}{N(T-c)} \sum_{t=c}^{T-1} \sum_{i=0}^{N-1} \|\mathbf{x}_i^t - \mathbf{y}_i^t\|_2$ and FDE as $FDE(\mathbf{x}^{c:T}, \mathbf{y}^{c:T}) = \frac{1}{N} \sum_{i=0}^{N-1} \|\mathbf{x}_i^{T-1} - \mathbf{y}_i^{T-1}\|_2$. For probabilistic models, the mean ADE and FDE of 5 runs is reported.

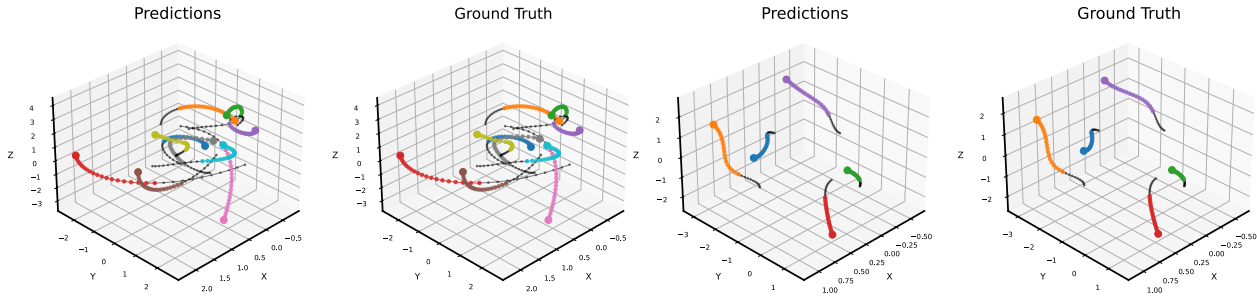


Figure 3: Inference results on N-Body Gravity (*left*) and Charged (*right*). The black dots represent the 10 conditioning steps, the colored dots are the 20 generated steps.

Implementation We process the particles as fully connected dynamic graphs, where each particle at each timestep is represented with a node. In case of STFlow, the node features consist of position, velocity and velocity magnitude, as well as acceleration and acceleration magnitude; the edge features contain Euclidean distance, relative position and relative velocity. In the Spring setting, a value of 0 or 1 is added as edge feature indicating a spring and in the Charged setting the charge is added as node feature, which are also used in the baselines. We predict a vector field on the velocities, use 3 layers of STFlow with a hidden dimension of 64, use 50 number of function evaluations during inference and use data augmentation during training by random rotation along the three axes.

Results The results are shown in Table 1 and a visualization of Gravity and Charged simulations can be seen in Figure 3. STFlow produces lower errors compared to all other models, where the biggest difference can be seen in the FDE metric. The performance increase compared to the previous best evaluated model, GeoTDM, is on average 54.6% for ADE and 62.8% for FDE. The trajectory-based approaches, which predict a longer time frame at once instead of using an autoregressive approach, produce better results, likely due to avoiding error accumulation during rollout.

4.1.2 MD17

Datasets and setup For the simulation of molecule trajectories we evaluate on the MD17 dataset (Chmiela et al., 2017). The dataset contains 8 small molecules from which positions over time have been simulated in one long trajectory using Density Functional Theory (Kohn et al., 1996). Each molecule has 9 (Ethanol, Malonaldehyde) to 21 (Aspirin) atoms and each molecule has a different trajectory length. We subsample by keeping 1 out of every 10 frames as in Han et al. (2024) and use a training/validation/test split of 70/15/15, split along the time axis. Trajectory lengths are $T = 30$ with $c = 10$ and a step size of 10 frames is used to sample the trajectories. The same baselines and metrics as the N-body experiments are used here.

Implementation We again use a fully connected graph, as the number of nodes is small, instead of using n -hop connectivity. We predict a vector field on the atom velocities. As node features we add a one hot encoding representing the atom type. We do not use any additional edge features. We use 3 layers of STFlow with a hidden dimension of 64, use 50 NFE during inference and use data augmentation during training by random rotation along the three axis.

Results The results can be seen in Table 3. STFlow produces the lowest errors across all 8 molecules, with an average improvement of 38.7% ADE and 34.1% FDE compared to GeoTDM, the second-best scoring model for all molecules. This shows that our model is capable of learning complex conditional geometric trajectory distributions.

4.1.3 Pedestrian trajectory forecasting

Datasets and setup Lastly, we also evaluate on the forecasting of pedestrian trajectories from the widely used ETH-UCY dataset (Pellegrini et al., 2009; Lerner et al., 2007). The dataset contains five different scenes named ETH, Hotel, Univ, Zara1 and Zara2. We use the common setup of $c = 8$ condition frames (3.2s) and $f = 12$ prediction frames (4.8s) (Xu et al., 2022). We use a leave-one-out evaluation by training on all scenes except one and then evaluate on the left out scene, which is repeated for all scenes. The training/validation split is 85/15.

Baselines The baseline approaches consist of generative models specifically made for pedestrian forecasting, namely: SGAN (Gupta et al., 2018) (GAN); PECNet (Mangalam et al., 2020), Traj++ (Salzmann et al., 2021), BiTraP (Yao et al., 2020), SVAE (Xu et al., 2022) (VAEs); and MID (Gu et al., 2022b). Additionally, we consider GeoTDM (Han et al., 2024) as a diffusion-based baseline for general stochastic trajectory simulation.

Metrics Instead of using the mean of 5 inference rollouts per test sample, it is standard in pedestrian forecasting literature to evaluate on the minimum ADE and minimum FDE of 20 rollouts per test sample, which we follow in this evaluation.

Implementation Pedestrians and their interactions are represented using a radius graph with $r = 8$ meters, with a maximum of 10 edges per node to avoid large memory requirements, where there is a node for each pedestrian at each point in time. Node features are 2D positions, velocity (magnitude), acceleration (magnitude) and a measure of local crowdedness. Edge features are Euclidean distance, relative position, relative velocity, relative turning angle and relative local crowdedness.

We predict a vector field of the pedestrian velocities using 1 layer of STFlow with a hidden dimension of 64, we use 50 NFE during inference and use data augmentation during training by random rotation along the two axes.

Results Looking at Table 2, we can see that STFlow achieves close to state-of-the-art performance on all scenes except one, and beats the best models in 2 out of 5 scenes. We noticed that, as the dataset contains relatively few unique trajectories, our model was prone to over-fitting on the training data. Although our approach was not specifically designed for pedestrian forecasting, its ability to achieve the lowest errors in some scenes establishes the broad capability and applicability of our model.

4.2 Density evaluation

As the goal of our model is to learn the distributions over the dynamics of diverse systems, we also compare the simulated and ground-truth densities over relevant features for the MD17 Ethanol test set results, shown in Figure 4. The velocity and acceleration densities produced by STFlow closely match the ground truth trajectory densities, showing that it has learned to statistically match the dynamics of the data and that it even generates rare events with the right relative frequencies, as demonstrated by the log-scale on the right hand side of Figure 4.

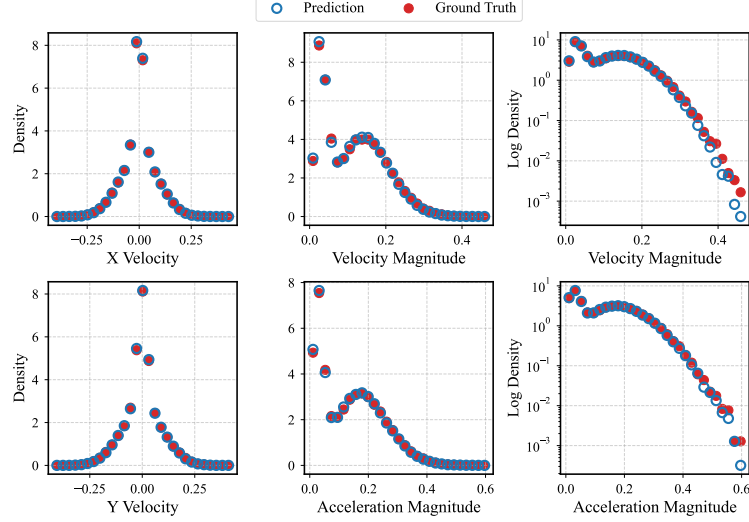


Figure 4: Velocity and acceleration density estimates from the 20 predicted frames of the MD17 Ethanol test set ($N = 216320$).

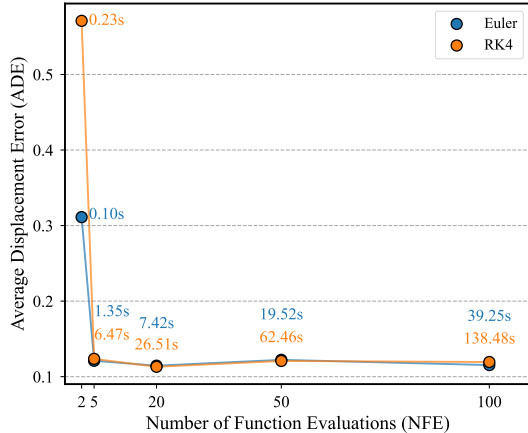


Figure 5: Performance and runtime evaluation of fixed timestep ODE solvers on 1000 samples from the Gravity test set. The numbers inside represent the runtime per batch of size 100 during inference.

4.3 Sampling efficiency

We also evaluate our model in terms of sampling efficiency during inference. Figure 5 shows the model’s performance on 1000 test samples of the Gravity dataset in terms of the mean ADE of 5 runs as well as the inference time required to simulate a single batch, for different amount of flow field integration steps using both an Euler and 4th order Runge-Kutta solver. We observe that performance saturates already when using only 5 integration steps (0.121 ADE). Compared to the diffusion approaches of (Han et al., 2024) and (Gu et al., 2022b), which use 100 or 1000 denoising steps, this is a significant improvement. This decrease in required sampling steps can be attributed to our use of coupled flow matching, enabling reduced transport cost between the prior and target distribution and consequently shorter and more straight flows than the more curved paths learned by diffusion models (Lipman et al., 2023).

4.4 Ablation study

In order to understand the contributions of the components to the performance of our model, we remove individual components and investigate the change in accuracy. Results are shown in Table 4; the ‘Baseline’ row denotes the performance when evaluating samples from the prior p_0 itself as model predictions.

Ablations on prior We look at three different ablations for the prior p_0 , namely an uninformed Gaussian $\mathcal{N}(\mathbf{0}, \mathbf{I})$, a Gaussian centered at the last conditioning frame $\mathcal{N}(\mathbf{x}_1^{c-1}, \mathbf{I})$ and a Gaussian random walk defined by Eq. 2, with a noise scaling parameter of $s = 1$ instead of $s = 4$. The two uninformed position-based priors ($\mathcal{N}(\mathbf{0}, \mathbf{I})$ and $\mathcal{N}(\mathbf{x}_1^{c-1}, \mathbf{I})$) consistently lead to increased errors, while performance is similar or better when using an informed random walk as prior. This aligns with our hypothesis that using a prior which incorporates trajectory-specific characteristics expedites learning and leads to better performance. We note that the displacement errors of the Ethanol dataset for p_0 with $s = 1$ are lower than that of our original approach. A possible explanation is that the target frames $\mathbf{x}_1^{c:T}$ in the Ethanol dataset may be more correlated with the conditioning frames $\mathbf{x}_1^{0:c}$ than in the Gravity dataset, making the prior with the higher amount of noise in the velocities perform worse. As such, s is an important hyperparameter that can be tuned for each dataset to further improve performance.

Ablations on model architecture We also removed the spatial message passing layer to confirm that our datasets contain crucial interactions and that our model can capture these interactions. This observation is backed by our ablation results, showing inferior performance when the model is unable to exchange information between other nodes in space. As the last ablation, we let \mathbf{x} and \mathcal{E} unchanged after each layer, decoding \mathbf{h} only after the final layer. This resulted in slightly worse performance, showing that our approach likely benefits from iteratively updating \mathcal{G} before predicting the final vector field.

5 Conclusion

We introduced STFlow, a novel flow matching model designed for probabilistic simulation of geometric trajectories in N-body systems. By uniquely leveraging data-dependent couplings and a physics-informed prior, STFlow effectively learns a map from the prior distribution to the intricate data distribution over system dynamics. Our approach not only respects fundamental permutation symmetries inherent in N-body problems but also demonstrably reduces prediction errors and enhances inference efficiency compared to existing methods. Evaluations across diverse benchmarks confirm STFlow’s state-of-the-art performance. The results highlight the significant benefits of incorporating domain-specific prior knowledge into deep generative models for complex trajectory simulations.

Table 4: Ablations. Metrics are ADE/FDE.

	Gravity	Ethanol
Baseline	1.591/3.101	0.512/0.845
STFlow $p_0, s = 4$ (2)	0.115/0.245	0.079/0.141
Prior		
$\mathcal{N}(\mathbf{0}, \mathbf{I})$	0.185/0.382	0.204/0.365
$\mathcal{N}(\mathbf{x}_1^{c-1}, \mathbf{I})$	0.169/0.353	0.198/0.357
$p_0, s = 1$ (2)	0.118/0.252	0.066/0.118
Architecture		
w/o Spatial layer	0.663/1.163	0.266/0.387
w/o Graph updating	0.128/0.272	0.090/0.158

Limitations and future work Our current approach is limited to equal-length trajectories per dataset. In case arbitrarily long trajectory simulation is required, decomposing the trajectories into smaller sections and using an autoregressive approach could be a viable solution. Additionally, the usage of a random walk as prior might be unsuitable for systems with highly oscillatory behaviors, strong external influences or hard constraints. In this case, more involved prior distributions designed by domain experts can straightforwardly be integrated into STFlow, as long as sampling from such priors remains efficient. Another relevant research direction is to further reduce the computational complexity and optimize simulation during inference by producing straighter flows (Yang et al., 2024). Additionally, the reformulation into a fully $E(n)$ -equivariant model could facilitate more efficient geometric learning (Klein et al., 2023). Finally, STFlow in principle already allows for generation of trajectories conditioned on arbitrary observed timesteps, and investigating the performance in this context is relevant for tasks that we did not consider in this work, e.g. endpoint-conditioned simulation, super-resolution, or imputation.

References

Michael S. Albergo, Mark Goldstein, Nicholas Matthew Boffi, Rajesh Ranganath, and Eric Vanden-Eijnden. Stochastic Interpolants with Data-Dependent Couplings. In *International Conference on Machine Learning (ICML)*, 2024.

Javad Amirian, Jean-Bernard Hayet, and Julien Pette. Social ways: Learning multi-modal distributions of pedestrian trajectories with gans. In *Proceedings of the IEEE/CVF Conference on Computer Vision and Pattern Recognition (CVPR) Workshops*, June 2019.

Peter Battaglia, Razvan Pascanu, Matthew Lai, Danilo Jimenez Rezende, and koray kavukcuoglu. Interaction networks for learning about objects, relations and physics. In D. Lee, M. Sugiyama, U. Luxburg, I. Guyon, and R. Garnett, editors, *Advances in Neural Information Processing Systems*, volume 29. Curran Associates, Inc., 2016. URL https://proceedings.neurips.cc/paper_files/paper/2016/file/3147da8ab4a0437c15ef51a5cc7f2dc4-Paper.pdf.

Erik J Bekkers, Sharvaree Vadgama, Rob Hesselink, Putri A Van der Linden, and David W. Romero. Fast, expressive $\mathcal{SE}(n)$ equivariant networks through weight-sharing in position-orientation space. In *The Twelfth International Conference on Learning Representations*, 2024. URL <https://openreview.net/forum?id=dPHLbUqGbr>.

Johannes Brandstetter, Rob Hesselink, Elise van der Pol, Erik J Bekkers, and Max Welling. Geometric and physical quantities improve $e(3)$ equivariant message passing, 2022a. URL <https://arxiv.org/abs/2110.02905>.

Johannes Brandstetter, Daniel E. Worrall, and Max Welling. Message passing neural PDE solvers. In *International Conference on Learning Representations*, 2022b. URL <https://openreview.net/forum?id=vSix3HPYKSU>.

Jeroen Bédorf. *The gravitational billion body problem*. PhD thesis, Faculty of Science, Leiden University, 2014.

Salva Rühling Cachay, Bo Zhao, Hailey Joren, and Rose Yu. DYffusion: A dynamics-informed diffusion model for spatiotemporal forecasting. In *Thirty-seventh Conference on Neural Information Processing Systems*, 2023. URL <https://openreview.net/forum?id=WRGldGm5Hz>.

Stefan Chmiela, Alexandre Tkatchenko, Huziel E. Sauceda, Igor Poltavsky, Kristof T. Schütt, and Klaus-Robert Müller. Machine learning of accurate energy-conserving molecular force fields. *Science Advances*, 3(5), May 2017. ISSN 2375-2548. doi: 10.1126/sciadv.1603015. URL <http://dx.doi.org/10.1126/sciadv.1603015>.

Miles Cranmer, Alvaro Sanchez Gonzalez, Peter Battaglia, Rui Xu, Kyle Cranmer, David Spergel, and Shirley Ho. Discovering symbolic models from deep learning with inductive biases. In H. Larochelle, M. Ranzato, R. Hadsell, M.F. Balcan, and H. Lin, editors, *Advances in Neural Information Processing Systems*, volume 33, pages 17429–17442. Curran Associates, Inc., 2020. URL https://proceedings.neurips.cc/paper_files/paper/2020/file/c9f2f917078bd2db12f23c3b413d9cba-Paper.pdf.

Carolina Cuesta-Lazaro and Siddharth Mishra-Sharma. Point cloud approach to generative modeling for galaxy surveys at the field level. *Physical Review D*, 109(12):123531, 2024.

Prafulla Dhariwal and Alex Nichol. Diffusion models beat gans on image synthesis, 2021. URL <https://arxiv.org/abs/2105.05233>.

Fabian B. Fuchs, Daniel E. Worrall, Volker Fischer, and Max Welling. Se(3)-transformers: 3d roto-translation equivariant attention networks, 2020. URL <https://arxiv.org/abs/2006.10503>.

Alessio Gravina and Davide Bacciu. Deep learning for dynamic graphs: models and benchmarks. *IEEE Transactions on Neural Networks and Learning Systems*, 2024.

Tianpei Gu, Guangyi Chen, Junlong Li, Chunze Lin, Yongming Rao, Jie Zhou, and Jiwen Lu. Stochastic trajectory prediction via motion indeterminacy diffusion. In *Proceedings of the IEEE/CVF Conference on Computer Vision and Pattern Recognition*, pages 17113–17122, 2022a.

Tianpei Gu, Guangyi Chen, Junlong Li, Chunze Lin, Yongming Rao, Jie Zhou, and Jiwen Lu. Stochastic trajectory prediction via motion indeterminacy diffusion, 2022b. URL <https://arxiv.org/abs/2203.13777>.

Agrim Gupta, Justin Johnson, Li Fei-Fei, Silvio Savarese, and Alexandre Alahi. Social gan: Socially acceptable trajectories with generative adversarial networks, 2018. URL <https://arxiv.org/abs/1803.10892>.

Jayesh Gupta, Sai Vemprala, and Ashish Kapoor. Learning modular simulations for homogeneous systems. In S. Koyejo, S. Mohamed, A. Agarwal, D. Belgrave, K. Cho, and A. Oh, editors, *Advances in Neural Information Processing Systems*, volume 35, pages 14852–14864. Curran Associates, Inc., 2022. URL https://proceedings.neurips.cc/paper_files/paper/2022/file/5f1b350fc0c2affd56f465faa36be343-Paper-Conference.pdf.

Jiaqi Han, Minkai Xu, Aaron Lou, Haotian Ye, and Stefano Ermon. Geometric Trajectory Diffusion Models. In *The Thirty-eighth Annual Conference on Neural Information Processing Systems*, 2024.

Douglas C. Heggie. The gravitational million-body problem. *Symposium - International Astronomical Union*, 208:81–92, 2003. doi: 10.1017/S0074180900207043.

Jonathan Ho, Ajay Jain, and Pieter Abbeel. Denoising diffusion probabilistic models. In H. Larochelle, M. Ranzato, R. Hadsell, M.F. Balcan, and H. Lin, editors, *Advances in Neural Information Processing Systems*, volume 33, pages 6840–6851. Curran Associates, Inc., 2020. URL <https://proceedings.neurips.cc/paper/2020/file/4c5bcfec8584af0d967f1ab10179ca4b-Paper.pdf>.

Jonathan Ho, William Chan, Chitwan Saharia, Jay Whang, Ruiqi Gao, Alexey Gritsenko, Diederik P. Kingma, Ben Poole, Mohammad Norouzi, David J. Fleet, and Tim Salimans. Imagen video: High definition video generation with diffusion models, 2022. URL <https://arxiv.org/abs/2210.02303>.

Emiel Hoogeboom, Alexey A. Gritsenko, Jasmijn Bastings, Ben Poole, Rianne van den Berg, and Tim Salimans. Autoregressive diffusion models. In *International Conference on Learning Representations*, 2022. URL <https://openreview.net/forum?id=Lm8T39vLDTE>.

Thomas Kipf, Ethan Fetaya, Kuan-Chieh Wang, Max Welling, and Richard Zemel. Neural relational inference for interacting systems, 2018. URL <https://arxiv.org/abs/1802.04687>.

Leon Klein, Andreas Krämer, and Frank Noe. Equivariant flow matching. In *Thirty-seventh Conference on Neural Information Processing Systems*, 2023. URL <https://openreview.net/forum?id=eLH2NF001B>.

Georg Kohl, Li-Wei Chen, and Nils Thuerey. Benchmarking autoregressive conditional diffusion models for turbulent flow simulation, 2024. URL <https://arxiv.org/abs/2309.01745>.

W. Kohn, A. D. Becke, and R. G. Parr. Density functional theory of electronic structure. *The Journal of Physical Chemistry*, 100(31):12974–12980, 1996. doi: 10.1021/jp9606691. URL <https://doi.org/10.1021/jp9606691>.

Pablo Lemos, Niall Jeffrey, Miles Cranmer, Shirley Ho, and Peter Battaglia. Rediscovering orbital mechanics with machine learning. *Machine Learning: Science and Technology*, 4(4):045002, oct 2023. doi: 10.1088/2632-2153/acfa63. URL <https://dx.doi.org/10.1088/2632-2153/acfa63>.

Alon Lerner, Yiorgos Chrysanthou, and Dani Lischinski. Crowds by example. *Computer Graphics Forum*, 26(3): 655–664, 2007. doi: <https://doi.org/10.1111/j.1467-8659.2007.01089.x>. URL <https://onlinelibrary.wiley.com/doi/abs/10.1111/j.1467-8659.2007.01089.x>.

Yaron Lipman, Ricky T. Q. Chen, Heli Ben-Hamu, Maximilian Nickel, and Matthew Le. Flow Matching for Generative Modeling. In *International Conference on Learning Representations (ICLR)*, 2023.

Phillip Lippe, Bas Veeling, Paris Perdikaris, Richard Turner, and Johannes Brandstetter. Pde-refiner: Achieving accurate long rollouts with neural pde solvers. In *Advances in Neural Information Processing Systems*, volume 36, pages 67398–67433. Curran Associates, Inc., 2023. URL https://proceedings.neurips.cc/paper_files/paper/2023/file/d529b943af3dba734f8a7d49efcb6d09-Paper-Conference.pdf.

Xiao Luo, Jingyang Yuan, Zijie Huang, Huiyu Jiang, Yifang Qin, Wei Ju, Ming Zhang, and Yizhou Sun. HOPE: High-order graph ODE for modeling interacting dynamics. In Andreas Krause, Emma Brunskill, Kyunghyun Cho, Barbara Engelhardt, Sivan Sabato, and Jonathan Scarlett, editors, *Proceedings of the 40th International Conference on Machine Learning*, volume 202 of *Proceedings of Machine Learning Research*, pages 23124–23139. PMLR, 23–29 Jul 2023. URL <https://proceedings.mlr.press/v202/luo23f.html>.

Xiao Luo, Yiyang Gu, Huiyu Jiang, Hang Zhou, Jinsheng Huang, Wei Ju, Zhiping Xiao, Ming Zhang, and Yizhou Sun. PGODE: Towards high-quality system dynamics modeling. In *Forty-first International Conference on Machine Learning*, 2024. URL <https://openreview.net/forum?id=jrE7geZekq>.

Kartikeya Mangalam, Harshayu Girase, Shreyas Agarwal, Kuan-Hui Lee, Ehsan Adeli, Jitendra Malik, and Adrien Gaidon. It is not the journey but the destination: Endpoint conditioned trajectory prediction, 2020. URL <https://arxiv.org/abs/2004.02025>.

Weibo Mao, Chenxin Xu, Qi Zhu, Siheng Chen, and Yanfeng Wang. Leapfrog diffusion model for stochastic trajectory prediction. In *Proceedings of the IEEE/CVF Conference on Computer Vision and Pattern Recognition*, pages 5517–5526, 2023.

Koen Minartz, Yoeri Poels, Simon M. Koop, and Vlado Menkovski. Equivariant Neural Simulators for Stochastic Spatiotemporal Dynamics. In *Conference on Neural Information Processing Systems (NeurIPS)*, 2023.

Koen Minartz, Fleur Hendriks, Simon Martinus Koop, Alessandro Corbetta, and Vlado Menkovski. Discovering interaction mechanisms in crowds via deep generative surrogate experiments. *Scientific Reports*, 15(1):10385, 2025.

Roozbeh Mottaghi, Hessam Bagherinezhad, Mohammad Rastegari, and Ali Farhadi. Newtonian scene understanding: Unfolding the dynamics of objects in static images. In *Proceedings of the IEEE Conference on Computer Vision and Pattern Recognition*, pages 3521–3529, 2016.

Chris Pedersen, Laure Zanna, and Joan Bruna. Thermalizer: Stable autoregressive neural emulation of spatiotemporal chaos, 2025. URL <https://arxiv.org/abs/2503.18731>.

S. Pellegrini, A. Ess, K. Schindler, and L. van Gool. You’ll never walk alone: Modeling social behavior for multi-target tracking. In *2009 IEEE 12th International Conference on Computer Vision*, pages 261–268, 2009. doi: 10.1109/ICCV.2009.5459260.

David Ruhe, Johannes Brandstetter, and Patrick Forré. Clifford group equivariant neural networks. In *Thirty-seventh Conference on Neural Information Processing Systems*, 2023. URL <https://openreview.net/forum?id=n84bzMrGUD>.

David Ruhe, Jonathan Heek, Tim Salimans, and Emiel Hoogeboom. Rolling diffusion models. In Ruslan Salakhutdinov, Zico Kolter, Katherine Heller, Adrian Weller, Nuria Oliver, Jonathan Scarlett, and Felix Berkenkamp, editors, *Proceedings of the 41st International Conference on Machine Learning*, volume 235 of *Proceedings of Machine Learning Research*, pages 42818–42835. PMLR, 21–27 Jul 2024. URL <https://proceedings.mlr.press/v235/ruhe24a.html>.

David Salinas, Valentin Flunkert, Jan Gasthaus, and Tim Januschowski. Deepar: Probabilistic forecasting with autoregressive recurrent networks. *International Journal of Forecasting*, 36(3):1181–1191, 2020. ISSN 0169-2070. doi: <https://doi.org/10.1016/j.ijforecast.2019.07.001>. URL <https://www.sciencedirect.com/science/article/pii/S0169207019301888>.

Tim Salzmann, Boris Ivanovic, Punarjay Chakravarty, and Marco Pavone. Trajectron++: Dynamically-feasible trajectory forecasting with heterogeneous data, 2021. URL <https://arxiv.org/abs/2001.03093>.

Alvaro Sanchez-Gonzalez, Jonathan Godwin, Tobias Pfaff, Rex Ying, Jure Leskovec, and Peter Battaglia. Learning to simulate complex physics with graph networks. In Hal Daumé III and Aarti Singh, editors, *Proceedings of the 37th International Conference on Machine Learning*, volume 119 of *Proceedings of Machine Learning Research*, pages 8459–8468. PMLR, 13–18 Jul 2020. URL <https://proceedings.mlr.press/v119/sanchez-gonzalez20a.html>.

Victor Garcia Satorras, Emiel Hoogeboom, and Max Welling. E(n) Equivariant Graph Neural Networks. In *International Conference on Machine Learning (ICML)*, pages 9323–9332, 2021.

Youssef Shehata, Benjamin Holzschuh, and Nils Thuerey. Improved sampling of diffusion models in fluid dynamics with tweedie’s formula. In *The Thirteenth International Conference on Learning Representations*, 2025. URL <https://openreview.net/forum?id=0FbzC7B9xI>.

Aliaksandra Shysheya, Cristiana Diaconu, Federico Bergamin, Paris Perdikaris, José Miguel Hernández-Lobato, Richard E. Turner, and Emile Mathieu. On conditional diffusion models for pde simulations. In A. Globerson, L. Mackey, D. Belgrave, A. Fan, U. Paquet, J. Tomczak, and C. Zhang, editors, *Advances in Neural Information Processing Systems*, volume 37, pages 23246–23300. Curran Associates, Inc., 2024. URL https://proceedings.neurips.cc/paper_files/paper/2024/file/2974844555dc383ea16c5f35833c7a57-Paper-Conference.pdf.

Jascha Sohl-Dickstein, Eric Weiss, Niru Maheswaranathan, and Surya Ganguli. Deep unsupervised learning using nonequilibrium thermodynamics. In Francis Bach and David Blei, editors, *Proceedings of the 32nd International Conference on Machine Learning*, volume 37 of *Proceedings of Machine Learning Research*, pages 2256–2265, Lille, France, 07–09 Jul 2015. PMLR. URL <https://proceedings.mlr.press/v37/sohl-dickstein15.html>.

Nathaniel Thomas, Tess Smidt, Steven Kearnes, Lusann Yang, Li Li, Kai Kohlhoff, and Patrick Riley. Tensor field networks: Rotation-and translation-equivariant neural networks for 3d point clouds. *arXiv preprint arXiv:1802.08219*, 2018a.

Nathaniel Thomas, Tess E. Smidt, Steven Kearnes, Lusann Yang, Li Li, Kai Kohlhoff, and Patrick Riley. Tensor field networks: Rotation- and translation-equivariant neural networks for 3d point clouds. *CoRR*, abs/1802.08219, 2018b. URL <http://arxiv.org/abs/1802.08219>.

Aidan P. Thompson, H. Metin Aktulga, Richard Berger, Dan S. Bolintineanu, W. Michael Brown, Paul S. Crozier, Pieter J. in 't Veld, Axel Kohlmeyer, Stan G. Moore, Trung Dac Nguyen, Ray Shan, Mark J. Stevens, Julien Tranchida, Christian Trott, and Steven J. Plimpton. Lammps - a flexible simulation tool for particle-based materials modeling at the atomic, meso, and continuum scales. *Computer Physics Communications*, 271:108171, 2022. ISSN 0010-4655. doi: <https://doi.org/10.1016/j.cpc.2021.108171>. URL <https://www.sciencedirect.com/science/article/pii/S0010465521002836>.

Alexander Tong, Nikolay Malkin, G. Huguet, Yanlei Zhang, Jarrid Rector-Brooks, Kilian Fatras, Guy Wolf, and Y. Bengio. Improving and Generalizing Flow-Based Generative Models with Minibatch Optimal Transport. In *ICML Workshop on New Frontiers in Learning, Control, and Dynamical Systems*, 2023.

Aäron Van Den Oord, Nal Kalchbrenner, and Koray Kavukcuoglu. Pixel recurrent neural networks. In *International conference on machine learning*, pages 1747–1756. PMLR, 2016.

Haomin Wen, Youfang Lin, Yutong Xia, Huaiyu Wan, Qingsong Wen, Roger Zimmermann, and Yuxuan Liang. Diffstg: Probabilistic Spatio-Temporal Graph Forecasting with Denoising Diffusion Models. In *ACM SIGSPATIAL International Conference on Advances in Geographic Information Systems (GIS)*, pages 60:1–60:12, 2023.

Liming Wu, Zhichao Hou, Jirui Yuan, Yu Rong, and Wenbing Huang. Equivariant spatio-temporal attentive graph networks to simulate physical dynamics, 2024. URL <https://arxiv.org/abs/2405.12868>.

Chenxin Xu, Robby T. Tan, Yuhong Tan, Siheng Chen, Yu Guang Wang, Xinchao Wang, and Yanfeng Wang. Eqmotion: Equivariant multi-agent motion prediction with invariant interaction reasoning, 2023. URL <https://arxiv.org/abs/2303.10876>.

Pei Xu, Jean-Bernard Hayet, and Ioannis Karamouzas. *SocialVAE: Human Trajectory Prediction Using Timewise Latents*, page 511–528. Springer Nature Switzerland, 2022. ISBN 9783031197727. doi: 10.1007/978-3-031-19772-7_30. URL http://dx.doi.org/10.1007/978-3-031-19772-7_30.

Ling Yang, Zixiang Zhang, Zhilong Zhang, Xingchao Liu, Minkai Xu, Wentao Zhang, Chenlin Meng, Stefano Ermon, and Bin Cui. Consistency flow matching: Defining straight flows with velocity consistency, 2024. URL <https://arxiv.org/abs/2407.02398>.

Yu Yao, Ella Atkins, Matthew Johnson-Roberson, Ram Vasudevan, and Xiaoxiao Du. Bitrap: Bi-directional pedestrian trajectory prediction with multi-modal goal estimation, 2020. URL <https://arxiv.org/abs/2007.14558>.

Cagatay Yildiz, Melih Kandemir, and Barbara Rakitsch. Learning interacting dynamical systems with latent gaussian process ODEs. In Alice H. Oh, Alekh Agarwal, Danielle Belgrave, and Kyunghyun Cho, editors, *Advances in Neural Information Processing Systems*, 2022. URL <https://openreview.net/forum?id=v1bxRZJ9c8V>.

A Technical Appendices and Supplementary Material

A.1 Detailed training and inference procedures

The training and inference algorithms describing our approach are denoted below in Algorithm 1 and Algorithm 2.

Algorithm 1 Conditional Flow Matching Training

Require: Train Dataset p_1 , Model $v_\theta(\mathbf{x}, \mathbf{h}, \mathcal{E}, \tau)$

```

while Training do
     $\mathbf{x}_1 \sim p_1, \tau \sim \mathcal{U}[0, 1]$                                  $\triangleright$  Sample batch  $\mathbf{x}_1$  and denoising level  $\tau$ 
     $\mathbf{x}_0^{0:c} \leftarrow \mathbf{x}_1^{0:c}, \mathbf{x}_0^{c:T} \leftarrow \zeta(\mathbf{x}_1^{0:c})$      $\triangleright$  Make informed prior  $\mathbf{x}_0$  from observed frames  $\mathbf{x}_1^{0:c}$ 
     $\mathbf{x}_\tau \sim p_\tau = \mathcal{N}(\tau \mathbf{x}_1 + (1 - \tau) \mathbf{x}_0, \sigma_p^2)$      $\triangleright$  Sample trajectories from Gaussian probability path
     $u \leftarrow \mathbf{x}_1 - \mathbf{x}_0$                                           $\triangleright$  Calculate true vector field
     $\mathbf{h} \leftarrow \text{Features}(\mathbf{x}_\tau), \mathcal{E} \leftarrow \text{Connectivity}(\mathbf{x}_\tau)$      $\triangleright$  Construct geometric trajectory
     $v_\theta \leftarrow v_\theta(\mathbf{x}_\tau, \mathbf{h}, \mathcal{E}, \tau)$                                  $\triangleright$  Forward pass
     $\mathcal{L}_{CFM}(\theta) \leftarrow \|v_\theta - u\|^2$                                  $\triangleright$  Calculate loss
     $\theta \leftarrow \theta + \alpha \nabla_\theta \mathcal{L}_{CFM}(\theta)$                                  $\triangleright$  Backpropagate and optimize
end while

```

Algorithm 2 Inference using Euler Integration

Require: Test Dataset p_1 , Trained model $v_\theta(\mathbf{x}, \mathbf{h}, \mathcal{E}, \tau)$, Number of Function Evaluations n

```

for  $\mathbf{x}_1 \in p_1$  do
     $\mathbf{x}_0^{0:c} \leftarrow \mathbf{x}_1^{0:c}, \mathbf{x}_0^{c:T} \leftarrow \zeta(\mathbf{x}_1^{0:c})$      $\triangleright$  Make informed prior  $\mathbf{x}_0$  from observed frames  $\mathbf{x}_1^{0:c}$ 
     $\hat{\mathbf{x}} \leftarrow \mathbf{x}_0, \Delta\tau \leftarrow \frac{1}{n}$ 
    for  $\tau \in [0, \frac{1}{n}, \dots, \frac{n-1}{n}]$  do
         $\mathbf{h} \leftarrow \text{Features}(\hat{\mathbf{x}}), \mathcal{E} \leftarrow \text{Connectivity}(\hat{\mathbf{x}})$      $\triangleright$  Construct geometric trajectory
         $v_\theta \leftarrow v_\theta(\hat{\mathbf{x}}, \mathbf{h}, \mathcal{E}, \tau)$                                  $\triangleright$  Forward pass
         $\hat{\mathbf{x}} \leftarrow \hat{\mathbf{x}} + \Delta\tau \cdot v_\theta$                                  $\triangleright$  Update  $\hat{\mathbf{x}}$  using Euler method
    end for
end for

```

A.2 Definitions of EGCL and the UNet

Our Spatial Message Passing layer is based on the Equivariant Graph Convolutional Layer (Satorras et al., 2021), which we define as:

$$\begin{aligned}
 \mathbf{m}_{ij} &= \varphi_{\mathbf{m}}(\mathbf{h}_i, \mathbf{h}_j, \mathbf{e}_{ij}, \|\mathbf{x}_i - \mathbf{x}_j\|^2, \tau_{\text{emb}}, t_{\text{emb}}), \\
 \mathbf{h}'_i &= \text{LayerNorm} \left(\varphi_{\mathbf{h}} \left(\mathbf{h}_i, \tau_{\text{emb}}, \sum_{j \in \mathcal{N}(i)} \mathbf{m}_{ij} \right) + \mathbf{h}_i \right), \\
 \mathbf{x}'_i &= \mathbf{x}_i + \frac{1}{|\mathcal{N}(i)|} \sum_{j \in \mathcal{N}(i)} \varphi_{\mathbf{x}}(\mathbf{m}_{ij})(\mathbf{x}_i - \mathbf{x}_j),
 \end{aligned}$$

where $\varphi_{\mathbf{m}}, \varphi_{\mathbf{h}}, \varphi_{\mathbf{x}}$ are 2-layer MLPs with SiLU activation functions and $\tau_{\text{emb}}, t_{\text{emb}}$ are sinusoidal embeddings with 16 dimensions based on τ and timestep number t .

Our Temporal Convolution layer is based on the UNet design from Dhariwal and Nichol (2021), for which we use the following parameters in Table 5. The input of the UNet consists of a batch of \mathbf{h} and a sinusoidal embedding of τ of 16 dimensions. We convolve over the timestep axis, containing T frames for each trajectory. The output is the new \mathbf{h} and the change in the velocity vector field, $\Delta\mathbf{v}$, calculated using a 2-layer MLP $\varphi_{\mathbf{v}}(\mathbf{h})$.

Table 5: UNet parameters used in the Temporal Convolution layer

parameter	value
image_size	T
dims	1
in_channels	$h = 64$
model_channels	$h = 64$
out_channels	$h = 64$
num_res_blocks	2
channel_mult	(1,2)
num_heads	2
num_head_channels	$h = 64$
use_scale_shift_norm	True
resblock_updown	True
use_new_attention_order	True

A.3 Hyperparameters

The hyperparameters used to train and evaluate our model on every dataset are included in Table 6. As optimizer we used AdamW with default parameters in combination with a ReduceLROnPlateau based on minimum validation loss with factor 0.5 and a patience of 10. In Table 6, we specify how the connectivity of \mathcal{G} is determined, where k means k -nearest neighbors, and r means radius-based connectivity with a maximum distance of r . s is the parameter determining the amount of extra noise added in the informed prior by scaling the used variance of the velocities of the observed frames. We did not perform an automated hyperparameter search for optimal configurations, so improvements can be made with hyperparameter optimization.

Table 6: Training hyperparameters of all conditional generation experiments

	connectivity	#augmentations	#layers	τ distribution	s	lr	epochs	val/test	batch size
N-body									
Gravity	$k = 10$	8	3	$\sqrt{\mathcal{U}[0, 1]}$	4	$5 \cdot 10^{-4}$	200	0.15/0.15	32
Springs	$k = 5$	8	2	$\sqrt{\mathcal{U}[0, 1]}$	4	$5 \cdot 10^{-4}$	300	0.15/0.15	32
Charged	$k = 5$	8	3	$\mathcal{U}[0, 1]$	4	$5 \cdot 10^{-4}$	250	0.15/0.15	32
ETH-UCY									
ETH	$r = 8, k = 10$	2	1	$\sqrt{\mathcal{U}[0, 1]}$	4	$5 \cdot 10^{-4}$	100	0.1	16
Univ	$r = 8, k = 10$	4	1	$\sqrt{\mathcal{U}[0, 1]}$	4	$5 \cdot 10^{-4}$	150	0.1	32
Hotel	$r = 8, k = 10$	5	1	$\sqrt{\mathcal{U}[0, 1]}$	4	$5 \cdot 10^{-4}$	150	0.15	32
Zara1	$r = 8, k = 10$	5	1	$\sqrt{\mathcal{U}[0, 1]}$	4	$5 \cdot 10^{-4}$	150	0.15	32
Zara2	$r = 8, k = 10$	2	1	$\sqrt{\mathcal{U}[0, 1]}$	4	$5 \cdot 10^{-4}$	100	0.1	16
MD17									
Aspirin	$k = 22$	8	3	$\sqrt{\mathcal{U}[0, 1]}$	4	$5 \cdot 10^{-4}$	300	0.15/0.15	32
Benzene	$k = 22$	3	3	$\sqrt{\mathcal{U}[0, 1]}$	4	$5 \cdot 10^{-4}$	300	0.15/0.15	32
Ethanol	$k = 22$	4	3	$\sqrt{\mathcal{U}[0, 1]}$	4	$5 \cdot 10^{-4}$	300	0.15/0.15	32
Malonaldehyde	$k = 22$	2	3	$\sqrt{\mathcal{U}[0, 1]}$	4	$5 \cdot 10^{-4}$	300	0.15/0.15	32
Naphthalene	$k = 22$	6	3	$\sqrt{\mathcal{U}[0, 1]}$	4	$5 \cdot 10^{-4}$	300	0.15/0.15	32
Salicylic	$k = 22$	6	3	$\sqrt{\mathcal{U}[0, 1]}$	4	$5 \cdot 10^{-4}$	300	0.15/0.15	32
Toluene	$k = 22$	4	3	$\sqrt{\mathcal{U}[0, 1]}$	4	$5 \cdot 10^{-4}$	300	0.15/0.15	32
Uracil	$k = 22$	8	3	$\sqrt{\mathcal{U}[0, 1]}$	4	$5 \cdot 10^{-4}$	300	0.15/0.15	32

A.4 Compute resources

The hardware used for training the models is 1 compute node consisting of 72 CPU cores and an NVIDIA A100 with 40 GB of GPU memory. The total runtimes of each dataset for training on the train sets and running inference on the test sets are described in Table 7.

Table 7: Total training and inference times, rounded

	Training time (h)	Inference time (h)
N-body		
Gravity	12:00	01:00
Springs	08:00	00:40
Charged	10:30	01:10
ETH-UCY		
ETH	00:30	00:02
Univ	01:10	00:30
Hotel	02:00	00:07
Zara1	04:00	00:26
Zara2	01:00	00:18
MD17		
Aspirin	12:30	00:14
Benzene	09:00	00:34
Ethanol	08:00	00:29
Malonaldehyde	08:50	00:51
Naphthalene	13:00	00:20
Salicylic	11:10	00:19
Toluene	10:15	00:25
Uracil	04:30	00:07

A.5 Standard deviations

The means and standard deviations of the 5 runs for each dataset in the N-body simulation and MD17 datasets are denoted in Table 8 and 9.

Table 8: Conditional Generation on N-Body systems, averaged over 5 runs, with standard deviations

	Gravity		Spring		Charged	
	ADE	FDE	ADE	FDE	ADE	FDE
STFlow	0.115 ± 0.020	0.245 ± 0.050	0.0002 ± 0.00004	0.0004 ± 0.00009	0.093 ± 0.016	0.172 ± 0.034

Table 9: Conditional Generation of atom trajectories from MD17 dataset, averaged over 5 runs, with standard deviations.

	Aspirin		Benzene		Ethanol		Malonaldehyde	
	ADE	FDE	ADE	FDE	ADE	FDE	ADE	FDE
STFlow	0.086 ± 0.008	0.158 ± 0.018	0.014 ± 0.002	0.022 ± 0.003	0.079 ± 0.012	0.141 ± 0.025	0.076 ± 0.012	0.138 ± 0.026
Naphthalene								
	ADE	FDE	ADE	FDE	ADE	FDE	ADE	FDE
STFlow	0.023 ± 0.002	0.038 ± 0.004	0.043 ± 0.004	0.072 ± 0.009	0.036 ± 0.004	0.059 ± 0.008	0.058 ± 0.004	0.090 ± 0.010
Salicylic								
	ADE	FDE	ADE	FDE	ADE	FDE	ADE	FDE
STFlow	0.023 ± 0.002	0.038 ± 0.004	0.043 ± 0.004	0.072 ± 0.009	0.036 ± 0.004	0.059 ± 0.008	0.058 ± 0.004	0.090 ± 0.010
Toluene								
	ADE	FDE	ADE	FDE	ADE	FDE	ADE	FDE
STFlow	0.023 ± 0.002	0.038 ± 0.004	0.043 ± 0.004	0.072 ± 0.009	0.036 ± 0.004	0.059 ± 0.008	0.058 ± 0.004	0.090 ± 0.010
Uracil								
	ADE	FDE	ADE	FDE	ADE	FDE	ADE	FDE
STFlow	0.023 ± 0.002	0.038 ± 0.004	0.043 ± 0.004	0.072 ± 0.009	0.036 ± 0.004	0.059 ± 0.008	0.058 ± 0.004	0.090 ± 0.010

A.6 Additional plots

We provide additional plots of trajectories from the N-body, pedestrian datasets and MD17 datasets in Figure 8, 9, 10, 11, 12, 13, 14, 15, 16, 17. As well as additional density evaluation on the Gravity and Univ test sets in Figures 6 and 7.

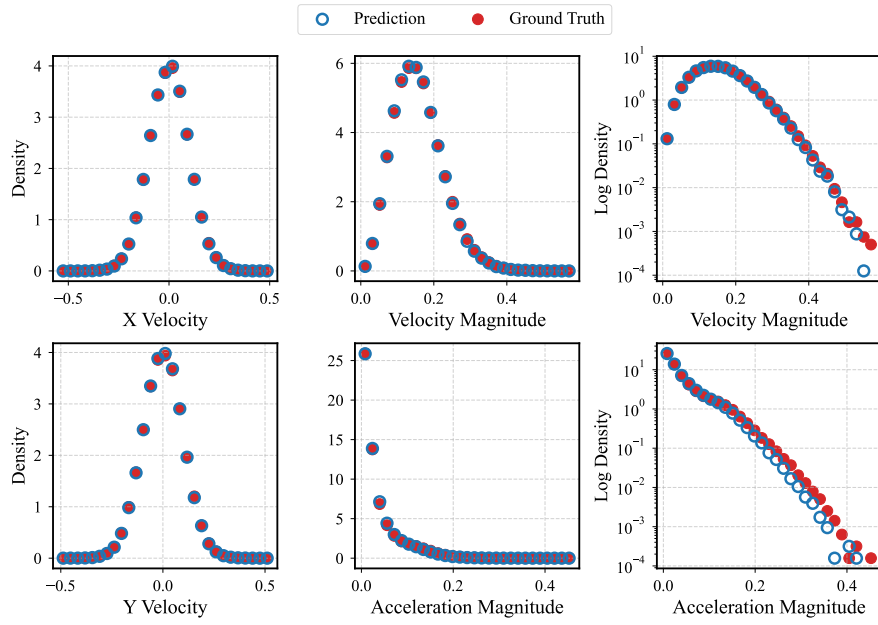


Figure 6: Density evaluation of velocities and accelerations from the Gravity test set inference trajectories

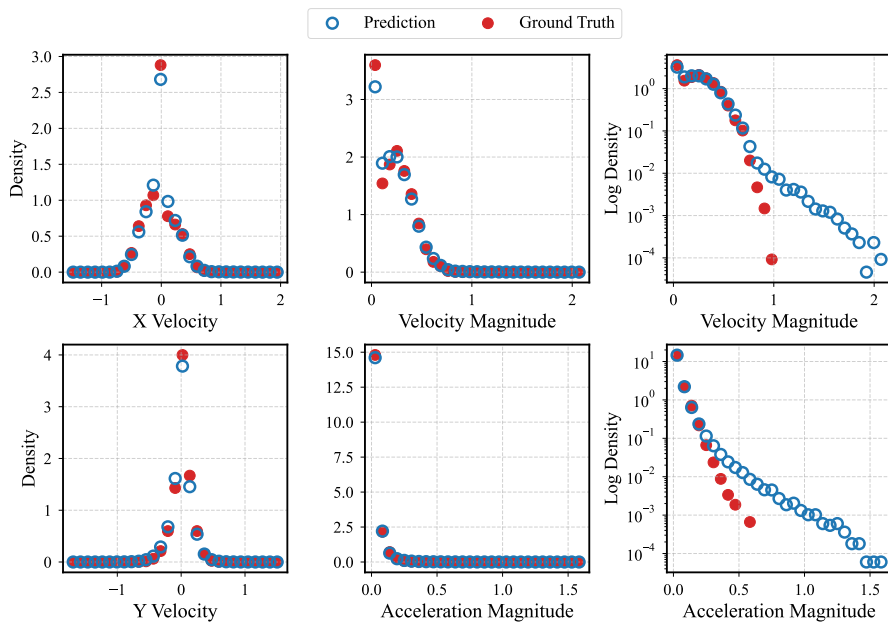


Figure 7: Density evaluation of velocities and accelerations from the ETH-UCY Univ test set inference trajectories

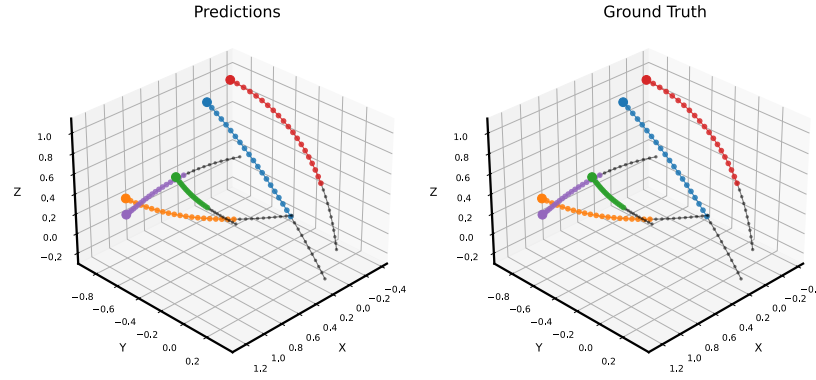


Figure 8: Trajectory inference results from the N-body Springs test set

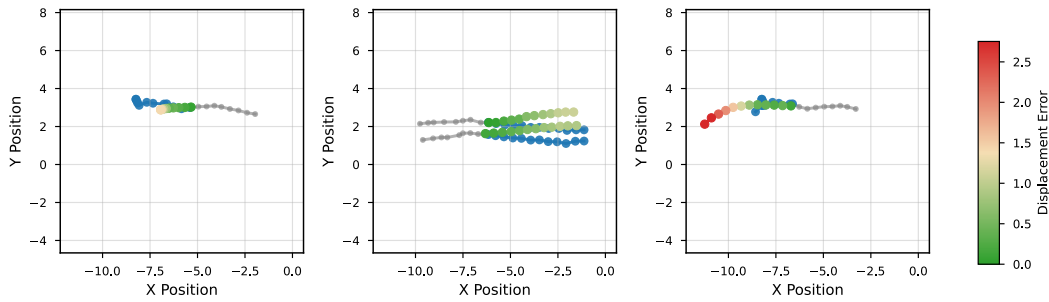


Figure 9: Three examples from the ETH Pedestrian trajectory inference runs

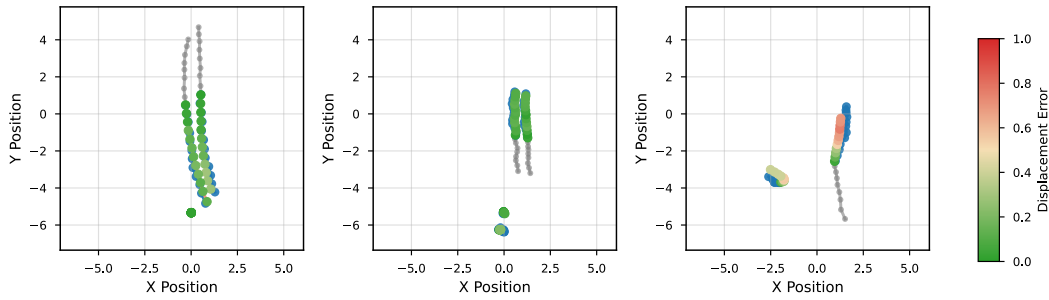


Figure 10: Three examples from the Hotel Pedestrian trajectory inference runs

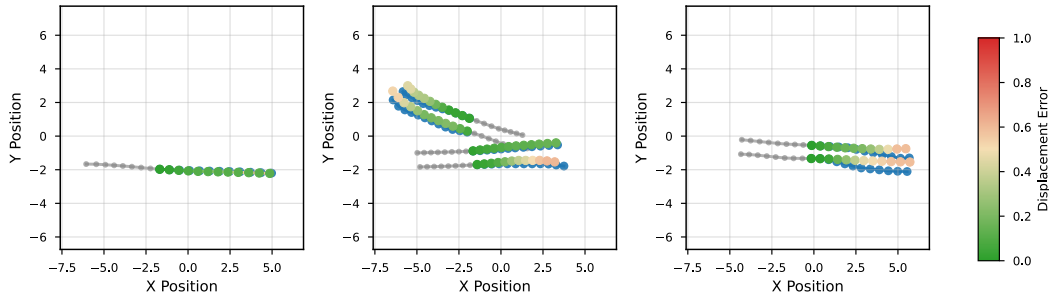


Figure 11: Three examples from the Zara01 Pedestrian trajectory inference runs

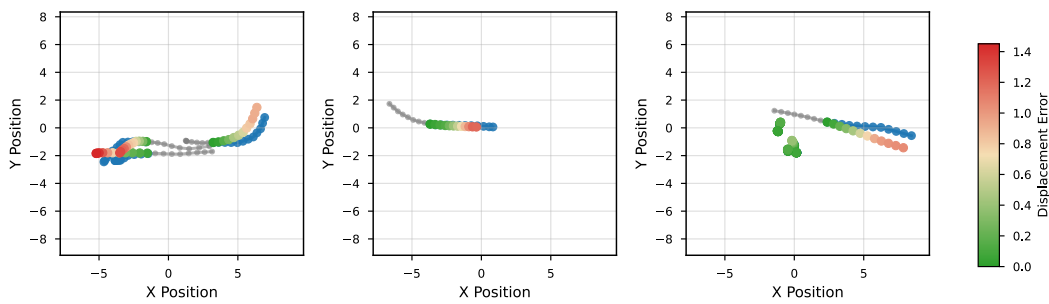


Figure 12: Three examples from the Zara02 Pedestrian trajectory inference runs

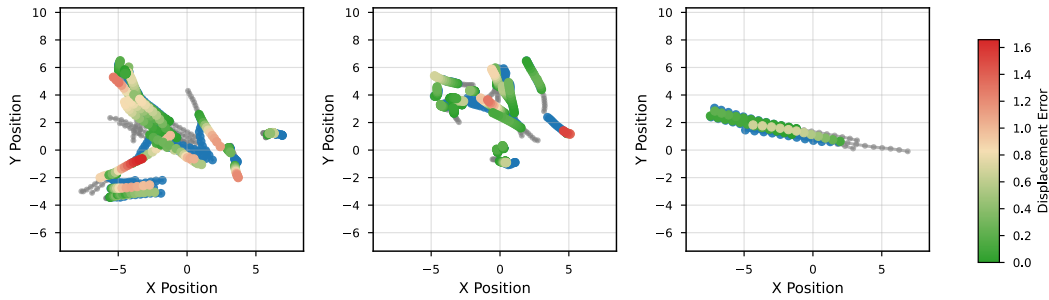


Figure 13: Three examples from the Univ Pedestrian trajectory inference runs

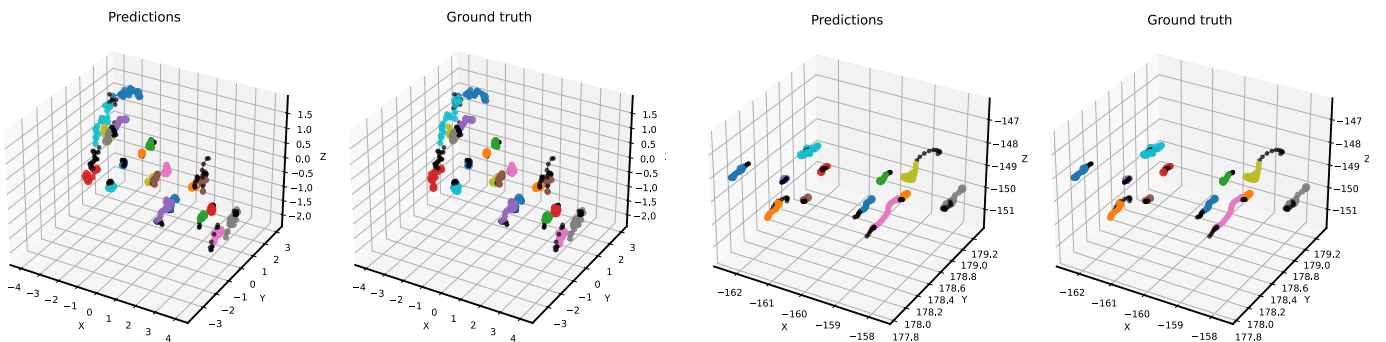


Figure 14: Aspirin (left) and Benzene (right) trajectory inference results from the MD17 test set

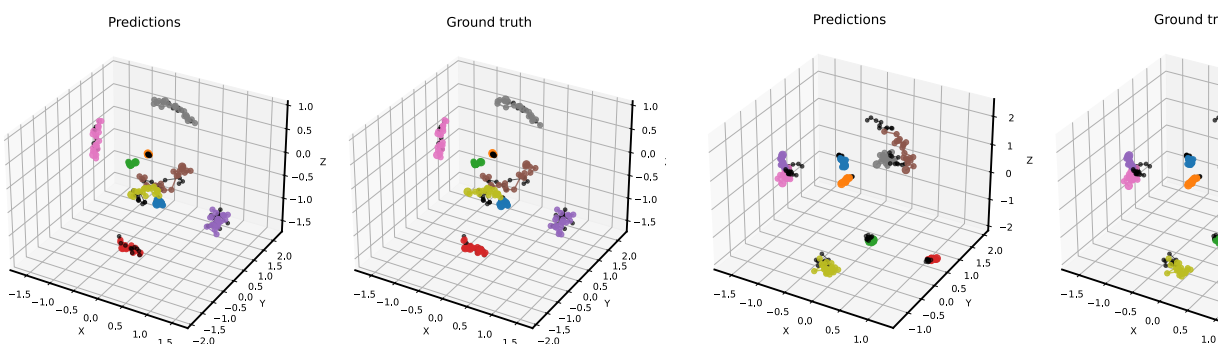


Figure 15: Ethanol (left) and Malonaldehyde (right) trajectory inference results from the MD17 test set

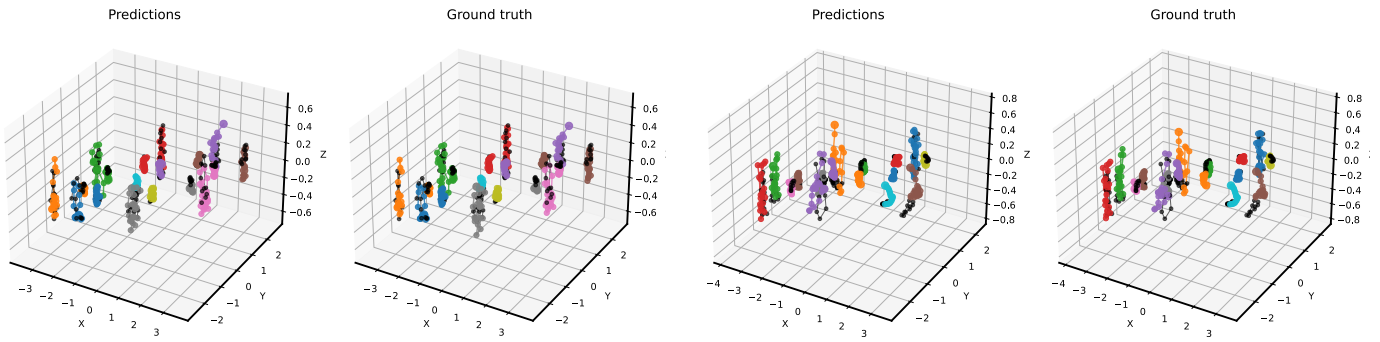


Figure 16: Naphthalene (left) and Salicylic (right) trajectory inference results from the MD17 test set

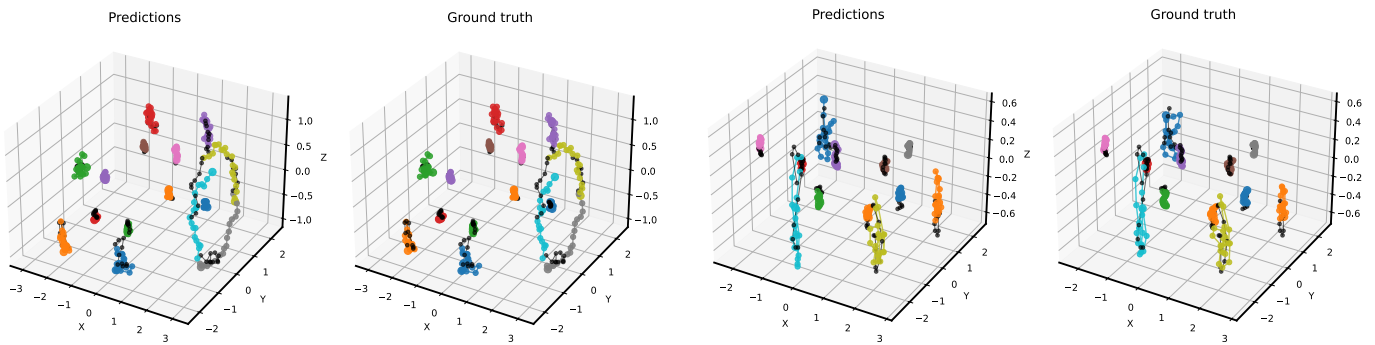


Figure 17: Toluene (left) and Uracil (right) trajectory inference results from the MD17 test set